

The evolution of the star formation activity per halo mass up to redshift ~ 1.6 as seen by Herschel \star

P. Popesso¹, A. Biviano², G. Rodighiero³, I. Baronchelli³, M. Salvato¹, A. Saintonge¹, A. Finoguenov¹, B. Magnelli¹, C. Gruppioni⁴, F. Pozzi⁵, D. Lutz¹, D. Elbaz⁶, B. Altieri⁷, P. Andreani^{8,2}, H. Aussel⁶, S. Berta¹, P. Capak^{9,10}, A. Cava¹¹, A. Cimatti⁵, D. Coia⁷, E. Daddi⁶, H. Dannerbauer⁶, M. Dickinson¹², K. Dasyra⁶, D. Fadda¹³, N. Förster Schreiber¹, R. Genzel¹, H.S. Hwang⁶, J. Kartaltepe¹², O. Ilbert¹⁴, E. Le Floch⁶, R. Leiton⁶, G. Magdis⁶, R. Nordon¹, S. Patel¹⁵, A. Poglitsch¹, L. Riguccini⁶, M. Sanchez Portal⁷, L. Shao¹, L. Tacconi¹, A. Tomczak¹⁶, K. Tran¹⁶, and I. Valtchanov⁷

¹ Max-Planck-Institut für Extraterrestrische Physik (MPE), Postfach 1312, 85741 Garching, Germany.

² INAF/Osservatorio Astronomico di Trieste, via G.B. Tiepolo 11, Trieste (Italy) I-34143

³ Dipartimento di Astronomia, Università di Padova, Vicolo dell'Osservatorio 3, 35122 Padova, Italy.

⁴ INAF-Osservatorio Astronomico di Bologna, via Ranzani 1, I-40127 Bologna, Italy.

⁵ Dipartimento di Astronomia, Università di Bologna, Via Ranzani 1, 40127 Bologna, Italy.

⁶ Laboratoire AIM, CEA/DSM-CNRS-Université Paris Diderot, IRFU/Service d'Astrophysique, Bât.709, CEA-Saclay, 91191 Gif-sur-Yvette Cedex, France.

⁷ Herschel Science Centre, European Space Astronomy Centre, ESA, Villanueva de la Cañada, 28691 Madrid, Spain

⁸ ESO, Karl-Schwarzschild-Str. 2, D-85748 Garching, Germany.

⁹ Spitzer Science Center, 314-6 Caltech, 1201 E. California Blvd. Pasadena, 91125

¹⁰ Department of Astronomy, 249-17 Caltech, 1201 E. California Blvd. Pasadena, 91125

¹¹ Departamento de Astrofísica, Facultad de CC. Físicas, Universidad Complutense de Madrid, E28040, Madrid, Spain

¹² National Optical Astronomy Observatory, 950 North Cherry Avenue, Tucson, AZ 85719, USA

¹³ NASA Herschel Science Center, Caltech 100-22, Pasadena, CA 91125, USA

¹⁴ Institute for Astronomy 2680 Woodlawn Drive Honolulu, HI 96822-1897, USA

¹⁵ Leiden Observatory, P.O. Box 9513 NL-2300 RA Leiden, The Netherlands

¹⁶ George P. and Cynthia W. Mitchell Institute for Fundamental Physics and Astronomy, Department of Physics and Astronomy, Texas A&M University, College Station, TX 77843

Received / Accepted

ABSTRACT

Aims. Star formation in massive galaxies is quenched at some point during hierarchical mass assembly. To understand where and when the quenching processes takes place, we study the evolution of the total star formation rate per unit total halo mass ($\Sigma(\text{SFR})/M$) in three different mass scales: low mass halos (field galaxies), groups, and clusters, up to a redshift $z \approx 1.6$.

Methods. We use deep far-infrared PACS data at 100 and 160 μm to accurately estimate the total star formation rate of the Luminous Infrared Galaxy population of 9 clusters with mass $\sim 10^{15} M_{\odot}$, and 9 groups/poor clusters with mass $\sim 5 \times 10^{13} M_{\odot}$. Estimates of the field $\Sigma(\text{SFR})/M$ are derived from the literature, by dividing the star formation rate density by the mean comoving matter density of the universe.

Results. The field $\Sigma(\text{SFR})/M$ increases with redshift up to $z \sim 1$ and it is constant thereafter. The evolution of the $\Sigma(\text{SFR})/M-z$ relation in galaxy systems is much faster than in the field. Up to redshift $z \sim 0.2$, the field has a higher $\Sigma(\text{SFR})/M$ than galaxy groups and galaxy clusters. At higher redshifts, galaxy groups and the field have similar $\Sigma(\text{SFR})/M$, while massive clusters have significantly lower $\Sigma(\text{SFR})/M$ than both groups and the field. There is a hint of a reversal of the SFR activity vs. environment at $z \sim 1.6$, where the group $\Sigma(\text{SFR})/M$ lies above the field $\Sigma(\text{SFR})/M-z$ relation. We discuss possible interpretations of our results in terms of the processes of downsizing, and star-formation quenching.

Key words. Galaxies: star formation - Galaxies: clusters: general - Galaxies: evolution - Galaxies: starburst

1. Introduction

The level of star formation (SF) activity in galaxy systems is known to be suppressed relative to the field. According to the well known morphology-density relation (Dressler 1980) and the star formation rate (SFR)-density relation (Hashimoto et al. 1998; Lewis et al. 2002; Gómez et al. 2003), in the local

Universe high density regions, like groups and clusters, host mostly early type galaxies characterized by a lower level of SF activity than field (mostly late-type) galaxies.

The environmental dependence of galaxy SFR may change with redshift, as galaxies in systems undergo significant evolution. In higher-redshift clusters, the fraction of blue galaxies is higher (the so-called 'Butcher-Oemler' effect Butcher & Oemler 1978, 1984; Pimbblet 2003), and so are the fractions of cluster galaxies with spectra characterized by young stellar populations (Dressler & Gunn 1983; Dressler et al. 1999; Poggianti et al. 1999) and the fraction of galaxies with late-type morphology

Send offprint requests to: Paola Popesso, popesso@mpe.mpg.de

* Herschel is an ESA space observatory with science instruments provided by European-led Principal Investigator consortia and with important participation from NASA.

(Dressler et al. 1997; Fasano et al. 2000; Postman et al. 2005; Smith et al. 2005). Higher- z clusters are also observed to contain a higher fraction of infrared (IR) emitting galaxies (the so called “IR Butcher-Oemler effect” Saintonge et al. 2008; Haines et al. 2009; Temporin et al. 2009), where most of the IR emission is powered by SF.

Given this evolution and the morphology- and SFR-density relations observed locally, it is clear that a quenching of the star formation activity of galaxies in dense environments is required since $z \sim 1-2$, and that this quenching process must act faster in galaxy systems than in the field. When and where this quenching process takes place, is still a matter of debate. SF quenching is generally assumed to occur within the cluster environment, where processes like ram pressure (Gunn & Gott 1972), cumulative galaxy-galaxy hydrodynamic/gravitational interactions (Park & Hwang 2009), strangulation (Larson et al. 1980), and galaxy harassment (Moore et al. 1996) are particularly effective. Indeed, Tran et al. (2009) observed a higher fraction of star forming galaxies in a supergroups at $z = 0.37$ with respect to clusters at the same redshift. It has however also been claimed that SF quenching of cluster galaxies occur in low-mass groups or large-scale filaments prior to cluster assembly (the so-called “pre-processing” Zabludoff & Mulchaey 1998; Kodama et al. 2001; Fadda et al. 2008; Porter et al. 2008; Balogh et al. 2011). The accretion process of groups onto clusters can itself lead to star-formation quenching (Poggianti et al. 2004), perhaps caused by rapid gas consumption due to a sudden enhancement of the SF activity (Miller & Owen 2003; Coia et al. 2005; Ferrari et al. 2005). It is also not clear whether environment plays any role at all in the quenching process. According to Peng et al. (2010), mass quenching is the dominant quenching process for massive galaxies, which generally reside in massive halos like groups and clusters. Since mass quenching should occur when a galaxy reaches a limiting mass, more massive galaxies, which reside in more massive halos, should be quenched earlier than less massive ones, having reached earlier the limiting mass for quenching. This creates an environment dependent quenching of galaxy SF, which is driven by some internal, rather than external, process, such as AGN feedback. This is supported observationally by the analysis of the star-formation histories of galaxies in the Virgo cluster region (Gavazzi et al. 2002), galaxies of higher H-band luminosities being characterized by shorter timescales of SF. Additional support to this scenario comes from the analysis of chemical abundances in elliptical galaxies by Pipino & Matteucci (2004).

Another way of looking at the evolution of the SF activity in galaxy systems is to consider a global quantity such as the star formation rate per unit of halo mass, that is the sum of the SFRs of all the galaxy in a system, divided by the system total mass, $\Sigma(\text{SFR})/M$. According to recent results (Kodama et al. 2004; Finn et al. 2004, 2005; Geach et al. 2006; Bai et al. 2009; Chung et al. 2010; Koyama et al. 2010; Hayashi et al. 2011), the evolution of the cluster $\Sigma(\text{SFR})/M$ is rapid, with a redshift dependence $\Sigma(\text{SFR})/M \propto (1+z)^\alpha$, with $\alpha \simeq 5-7$. The cluster $\Sigma(\text{SFR})/M$ evolves faster up to $z \sim 1$ than the fraction of IR-emitting galaxies (the IR Butcher-Oemler effect) because IR-emitting galaxies are not only more numerous in higher- z clusters but also more IR luminous, given the evolution of the cluster IR luminosity function (Bai et al. 2009). In addition, there are some indications that $\Sigma(\text{SFR})/M$ anti-correlates with halo mass in galaxy systems at similar redshift (Finn et al. 2004, 2005; Homeier et al. 2005; Koyama et al. 2010).

The quantity $\Sigma(\text{SFR})/M$ thus appears to be a powerful tool for analyzing the rapid evolution of galaxies in systems of dif-

ferent mass. To determine $\Sigma(\text{SFR})/M$ one needs to estimate the system dynamical mass and the SFRs of its member galaxies. Robust SFR estimates can be obtained from galaxy IR luminosities, L_{IR} , and these estimates are considered to be more reliable than the SFR based on optical emission-lines such as [OII] and H α (Geach et al. 2006).

If one considers only the systems where the total SFR has been derived from IR observations, the $\Sigma(\text{SFR})/M-z$ relation is currently based on ~ 15 galaxy clusters only (Biviano et al. 2011), all with masses¹ $M_{200} \gtrsim 10^{14} M_\odot$ and $z < 1$. Masses for these systems have been derived in different ways (from X-ray or lensing data, or from kinematical analyses of the population of cluster galaxies), and at different limiting radii.

The aim of this paper is to extend the study of the $\Sigma(\text{SFR})/M-z$ relation to systems of lower masses than clusters, and to higher z , with a homogeneous estimate of the system masses and total SFRs. Specifically, we extend the mass range down to the group mass regime, and to the typical dark matter halo mass of field galaxies ($10^{11} - 10^{12} M_\odot$). We also extend the redshift range up to $z \sim 1.6$. We use deep far-infrared PACS data at 100 and 160 μm to accurately estimate the total SFRs of 18 systems with masses in the range $2 \times 10^{13} - 3 \times 10^{15} M_\odot$, down to $L_{\text{IR}} = 10^{11} L_\odot$, i.e. the luminosity that characterizes the so-called Luminous IR Galaxies (LIRGs). This limit is set by the faintest luminosity observable with our data at $z \sim 1.6$. We use nearly complete galaxy spectroscopic samples to measure the system masses from their kinematics. To extend the $\Sigma(\text{SFR})/M-z$ relation to the field regime, i.e. to dark matter halo masses typical of field galaxies, we use published global SFR densities at different redshifts (Madau et al. 1998; Gruppioni et al. 2011; Magnelli et al. 2011).

In Sect. 2.1 and Sect. 2.2 we describe our sample and our spectroscopic and photometric data-set, in Sect. 2.3 we describe how we define system membership of the galaxies with available redshifts, and derive the system dynamical masses, in Sect. 2.4 we determine the total SFRs of the systems. The resulting $\Sigma(\text{SFR})/M-z$ relations are presented in Sect. 3 for clusters, groups (Sect. 3.1), and the field (Sect. 3.2). We summarize and discuss our results in Sect. 4.

We adopt $H_0 = 70 \text{ km s}^{-1} \text{ Mpc}^{-1}$, $\Omega_m = 0.3$, $\Omega_\Lambda = 0.7$ throughout this paper. We adopt a Salpeter IMF when calculating stellar masses and SFRs.

2. The data-set

2.1. The sample of galaxy systems

Our sample comprises 9 X-ray detected systems at $0.15 < z < 0.85$, all observed in the PACS Evolutionary Probe PACS GT Program (PEP, Lutz et al. 2011). The systems are listed in Table 1. In addition, we use the X-ray detected group and cluster catalog of the COSMOS field (Finoguenov et al., in prep.) to identify 27 systems at $z < 0.8$ with at least 10 spectroscopic members each, the minimum required for an acceptable mass estimate from the system kinematics (Girardi et al. 1993). The COSMOS field is observed as part of the PEP program. We further include in our sample 4 systems in the GOODS North and South fields at $0.7 < z < 1.6$ observed as part of the PACS GOODS-Herschel Program (Elbaz et al. 2011).

¹ The cluster virial mass, M_{200} , is the mass contained within a sphere of radius r_{200} , which is the radius within which the enclosed average mass density is 200 times the critical density. The two quantities are related by the expression $M_{200} \equiv 100 H(z)^2 r_{200}^3 / G$, where G is the gravitational constant and $H(z)$ the Hubble constant at the system redshift.

Of these systems, two are X-ray detected, one at $z = 0.73$ in GOODS-S (Gilli et al. 2003; Le Fèvre et al. 2004; Popesso et al. 2009), another one at $z = 1.02$ in GOODS-N (Elbaz et al. 2007), one system lies close to the Chandra CCD chip gap and it is not X-ray detected (GOODS-N system at $z = 0.85$ Bauer et al. 2002), and the highest redshift system (at $z = 1.612$) is only marginally X-ray detected in the Chandra GOODS-S map (Kurk et al. 2008). Finally, we include in our sample the Bullet cluster (Barrena et al. 2002; Markevitch et al. 2004), a well-known massive cluster undergoing a violent collision with an infalling group, which we use as a test-case for the dependence of the $\Sigma(\text{SFR})/M$ on the cluster dynamical state. PACS data for the Bullet cluster are not public yet. For this cluster we use the L_{IR} based on Spitzer MIPS $24 \mu\text{m}$ data published by Chung et al. (2010). The considered LIRGs members lie within 1.7 Mpc from the cluster center. This is close to the r_{200} radius, ~ 2 Mpc, estimated from the kinematics of cluster galaxies (Barrena et al. 2002).

We split our sample in groups and clusters depending on their mass estimates (see next section), groups/poor clusters with $10^{13} M_{\odot} < M_{200} < 3 \times 10^{14} M_{\odot}$ and clusters with $M_{200} \geq 3 \times 10^{14} M_{\odot}$. The mass value separating groups/poor clusters from clusters approximately corresponds to the richness class 0 in the catalog of Abell et al. (1989) (using the relations between mass and velocity dispersion and between velocity dispersion and richness class for galaxy clusters; see Girardi et al. 1993; Biviano et al. 2006).

2.2. Spectral and photometric data

We take the data for the COSMOS field from the multi-wavelength and IRAC-selected catalog of Ilbert et al. (2010) complemented with public Spitzer $24 \mu\text{m}$ (Le Flocc'h et al. 2009; Sanders et al. 2007) and PACS 100 and $160 \mu\text{m}$ data (Lutz et al. 2011). The association between $24 \mu\text{m}$ and PACS sources with their optical counterparts is done via a maximum likelihood method (see Lutz et al. 2011; Berta et al. 2010, for details). The photometric sources were cross-matched in coordinates with the sources for which a high-confidence spectroscopic redshift is available. For this purpose we use the public catalogs of spectroscopic redshifts complemented with other unpublished data. This catalog includes redshifts from either SDSS or the public zCOSMOS-bright data acquired using VLT/VIMOS (Lilly et al. 2007, 2009) complemented with Keck/DEIMOS (PIs: Scoville, Capak, Salvato, Sanders, Kartaltepe), Magellan/IMACS (Trump et al. 2007), and MMT (Prescott et al. 2006) spectroscopic redshifts.

Similar multi-wavelength (from UV to $24 \mu\text{m}$) data for the GOODS-S field is provided by the MUSIC catalog (Grazian et al. 2006; Santini et al. 2009) and complemented with PACS data at 70, 100 and $160 \mu\text{m}$ and spectroscopic redshifts from the PEP catalog (see Lutz et al. 2011 for more details) and from the GMASS survey (Cimatti et al. 2008).

We take the data for the GOODS-N field from the multi-wavelength catalog prepared by the PEP Team (Berta et al. 2010) including UV to MIPS 24 data, PACS 100 and $160 \mu\text{m}$ data, complemented with the spectroscopic redshift catalog of Barger et al. (2008).

We collect publicly available spectroscopic data for all clusters from the NED. For CL 0024+17 and MS 0451-03 we also collect multi-wavelength data from Moran et al. (2005, 2007). Multi-wavelength photometric data are not available for the other clusters. The references for each cluster spectroscopic sample are listed in Table 1. Each cluster sample is comple-

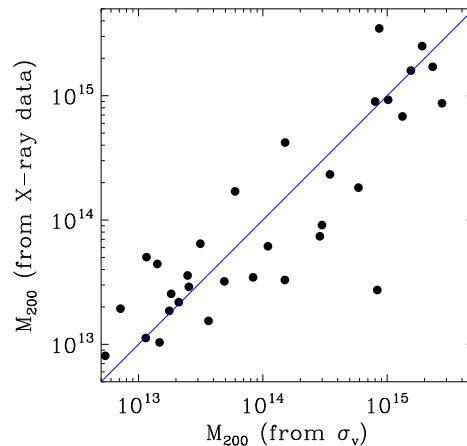


Fig. 1. Comparison of system mass estimates obtained from X-ray data with those obtained from system velocity dispersions.

mented with MIPS $24 \mu\text{m}$ data, when available, and PACS 100 and $160 \mu\text{m}$ data (Lutz et al. 2011).

The data reduction, source extraction, and a detailed explanation of the depths of the PACS maps used in this paper can be found in Lutz et al. (2011) and Elbaz et al. (2011), for the PEP and GOODS-Herschel surveys, respectively.

2.3. Membership and mass estimates of galaxy systems

To define the galaxies that are members of the systems described in Sect. 2.1, we adopt the algorithm of Mamon et al. (2010), which is based on the modeling of the mass and anisotropy profiles of cluster-sized halos extracted from a cosmological numerical simulation. This algorithm is more effective than traditional approaches (e.g. Yahil & Vidal 1977) in rejecting interlopers, while still preserving cluster members. The system membership selection depends on the location of galaxies in the system-centric distance – rest-frame velocity² diagram. The peaks of the X-ray surface brightness are adopted as centers of the X-ray detected systems. The galaxy number density maxima (estimated using an adaptive kernel technique) are adopted as centers for the other systems. The interloper rejection procedure is iterated until convergence.

As an outcome of the procedure of Mamon et al. (2010), the system dynamical masses are obtained from biweight estimates (Beers et al. 1990) of the system velocity dispersions along the line-of-sight, σ_v , as in Mauduit & Mamon (2007, see Appendix A). We use the σ_v -based mass estimates, rather than the more traditional virial mass estimates because the σ_v -based mass estimates are robust against problems of spatial incompleteness, unlike the more traditional virial theorem estimator (see Biviano et al. 2006), so we do not have to worry about the possibility that in some systems of our sample the spectroscopic completeness is different in different regions.

The uncertainties in the system mass estimates are estimated from the uncertainties in the biweight estimate of σ_v (Beers et al. 1990) via the propagation of error analysis.

² The galaxy rest-frame velocities with respect to the system mean velocity are obtained by the usual relation $v = c(z - \bar{z})/(1 + \bar{z})$ (Harrison & Noonan 1979), where \bar{z} is the system mean redshift, determined with the biweight estimator (Beers et al. 1990).

name	z	r_{200} (Mpc)	M_{200} ($10^{14} M_{\odot}$)	N_m	N_{LIRG}	% z_{spec}	ref
(1)	(2)	(3)	(4)	(5)	(6)	(7)	(8)
Cluster sample							
A2218	0.175	2.73	27.6	107	1	75%	1
A2219	0.226	2.375	19	126	2	68%	2
A2390	0.228	2.533	23	259	3	69%	3
MS 1358+62	0.329	1.711	8.2	286	1	73%	4
COSMOS_CL1 ^a	0.351	1.2	4.8	36	6	48%	5
MS 0451–03	0.539	1.966	15.5	342	8	80%	6
COSMOS_CL2 ^a	0.78	1.18	3.88	36	6	48%	5
MS 1054–03	0.830	1.521	10.1	134	5	100%	7
RX J0152–13	0.838	1.657	13.3	228	11	96%	8
Group/poor cluster sample							
COSMOS_GRI ^b	0.1	0.61	0.26	47	1	56%	5
COSMOS_GR2 ^b	0.22	0.62	0.31	77	1	66%	5
COSMOS_GR3 ^b	0.35	0.68	0.31	81	4	48%	5
CL 0024+17	0.395	0.96	1.5	396	10	92%	6,9
COSMOS_GR4 ^b	0.70	0.69	0.31	34	10	47%	5
GOODS – S_01	0.735	0.51	0.85	188	3	88%	10
GOODS – N_01	0.85	0.51	0.9	112	3	90%	11
GOODS – N_02	1.02	0.73	1.03	130	4	79%	11
GOODS – S_02	1.61	0.52	0.9	76	6	68%	10
Merging system							
Bullet cluster	0.297	1.7	9.5	43	5	–	12

Table 1. The table lists the following main properties of the cluster and group samples: column (1): name; column (2): redshift; column (3): radius r_{200} in Mpc; column (4): mass M_{200} in $10^{14} M_{\odot}$; column (5): number of members used in the estimate of M_{200} ; column (6): number of LIRG members within r_{200} ; column (7): spectroscopic completeness of the LIRG sample within r_{200} ; column (8): references for spectroscopic data: 1 Le Borgne et al. (1992); 2 SDSS DR7 (Abazajian et al. 2009); 3 Yee et al. (1996); 4 Fisher et al. (1998); 5 COSMOS spectroscopic sample, see text; 6 Moran et al. (2005); 7 Tran et al. (2007); 8 Patel et al. (2009); 9 Moran et al. (2007); 10 PEP-GOODS-S spectrophotometric catalog Popesso et al. (2011); 11 PEP-GOODS-N spectrophotometric catalog Berta et al. (2010); 12 Chung et al. (2010).

^a Composite of COSMOS clusters. The quantities reported for this system are the mean of the contributing systems.

^b Composite of COSMOS groups. The quantities reported for this system are the mean of the contributing systems.

As an alternative mass estimate we consider that obtained by assuming hydrostatic equilibrium of the X-ray-emitting intra-cluster or intra-group gas. The two mass-estimates are compared in Fig. 1 for those systems which have both estimates available. The scatter is large, but there is no significant bias, on average, between the two mass estimates. There is only one system for which the two mass estimates are in disagreement by more than 3σ . The discrepancy is probably due the low number of spectroscopic members (9) available for this system. We exclude it from our sample for further analyses.

2.4. Star formation rates

We fit the spectral energy distributions (SEDs) of all system members in our sample which have multiwavelength data available from the UV to the PACS wavelengths, using a set of empirical templates of local objects (Polletta et al. 2007; Gruppioni et al. 2010) that reproduce most of the observed galaxy SEDs from the optical to the FIR wavelengths (see Rodighiero et al. 2010). We then determine the galaxy L_{IR} by integrating the best-fit SED models from 8 to $1000 \mu\text{m}$.

We estimate the L_{IR} of those system members for which multiwavelength data are not available, by fitting their PACS data with SED models from Polletta et al. (2007), to extract the νL_{ν} at $100 \mu\text{m}$ rest frame, and by using the $L_{IR} - \nu L_{\nu}$ relation, as explained in Popesso et al. (in prep.).

Some of our member galaxies do not have PACS data either due to the incompleteness of the PACS photometric catalog between the 3 and 5σ levels, or because the PACS catalog are not deep enough to reach the required $10^{11} L_{\odot}$ limits at the redshift of the system. We determine the L_{IR} of these galaxies from their MIPS $24 \mu\text{m}$ flux densities by using the scaling relation of Chary & Elbaz (2001), corrected as explained in Popesso et al. (in prep.) to avoid overestimations (Elbaz et al. 2011; Nordon et al. 2011). We also re-determine in the same way the L_{IR} of the member galaxies of the Bullet cluster from the $24 \mu\text{m}$ data of Chung et al. (2010). In total, only 8 galaxies (9% of our member LIRGs) do not have their L_{IR} estimated from PACS data: 2 in MS 0451–03, 4 in RX J0152–13 and 2 in the $z \sim 1.6$ GOODS-S group.

The main advantage of using PACS data in the determination of the L_{IR} is to remove possible contamination by the emission of active galactic nuclei (AGN), since most of the rest-frame far-IR emission comes from the host galaxy (Netzer et al. 2007; Lutz et al. 2010). Thus, we do not need to exclude AGN hosts from our sample as was instead done in previous similar analysis (e.g. Geach et al. 2006; Bai et al. 2009; Biviano et al. 2011). AGN contamination is a concern, however, when estimating the SFR from $24 \mu\text{m}$ data. We do exclude the AGN hosts from the evaluation of the total SFR of the Bullet cluster, using the AGN classification of Chung et al. (2010), since PACS data are not yet publicly available for this cluster. We also cross-correlated the system members, whose L_{IR} is based

on 24 μm data only, with publicly available AGN catalogs (Johnson et al. 2003; Demarco et al. 2005; Brusa et al. 2009). None of those members turn out to be an AGN.

Finally, we estimate the galaxy SFRs from their L_{IR} via the law of Kennicutt (1999). The LIRG L_{IR} -limit corresponds to a limiting SFR of $17 M_{\odot} \text{ yr}^{-1}$.

We estimate $\Sigma(\text{SFR})$, the total SFR of each system, by summing up the SFRs of the LIRGs that are members of the system. We then correct $\Sigma(\text{SFR})$ for spectroscopic incompleteness in the following way. For all systems where the PACS data reach the $10^{11} L_{\odot}$ limit at the system redshift, we take as a reference the PACS 100 μm catalog. We plot the 100 μm flux density vs. L_{IR} of system member galaxies in narrow redshift bins to estimate the 100 μm flux density that corresponds to the LIRG L_{IR} at each redshift, $f_{\text{LIRG}}(z)$. The spectroscopic incompleteness is defined as the fraction of PACS sources with z , among all those with flux $> f_{\text{LIRG}}(z)$ within r_{200} . The inverse of this fraction is the correction factor that we apply to the $\Sigma(\text{SFR})$ estimates to correct for incompleteness. For the systems which contain member galaxies for which the L_{IR} -estimates are based on MIPS 24 μm flux densities, we use the same approach by using the 24 μm catalog as reference.

To test the reliability of this method, we consider a system with 100% spectroscopic completeness down to the LIR L_{IR} level, MS 1054–03 (Bai et al. 2009). We perform 500000 random extractions from the luminosity function of MS 1054–03 of a number of LIRGs corresponding to a given spectroscopic completeness. We repeat this test for all the spectroscopic coverage values listed in Table 1. We then estimate the uncertainty due to the incompleteness correction from the dispersion of the difference between the recovered $\Sigma(\text{SFR})$ and the real value. The uncertainty due to this correction is $\approx 20\%$ in the range of spectroscopic completeness of our sample.

The total uncertainty of the $\Sigma(\text{SFR})$ estimates is determined from the propagation of error analysis, by considering a 10% uncertainty in the L_{IR} estimates (see Lutz et al. 2011, for further details), and the 20% uncertainty due to the completeness correction.

The spectroscopic coverage of the COSMOS field is much lower than those of the clusters and GOODS fields and spatially not uniform. Thus, to reduce the error bars of the $\Sigma(\text{SFR})$, we combine the COSMOS groups and, separately, the COSMOS clusters in four, and, respectively, two redshift bins, see Table 1. In each z -bin we then define the mean $\Sigma(\text{SFR})$, M_{200} , and spectroscopic incompleteness, separately for the groups and the clusters contributing to the sample in that bin.

Counting the composite COSMOS groups and clusters as individual systems, our final sample comprises 9 massive clusters, 9 groups/poor clusters, and the Bullet cluster (see Table 1).

3. Results: the $\Sigma(\text{SFR})/M$ - z relation

3.1. Clusters versus groups

The $\Sigma(\text{SFR})/M$ -redshift relation is shown in Fig. 2. Black, and magenta symbols show the $\Sigma(\text{SFR})/M$ -redshift relation for the clusters and, respectively, the groups. For both samples there is evidence for a significant $\Sigma(\text{SFR})/M$ vs. z correlation, 99% significant according to a Spearman rank correlation test. On the other hand, we do not find evidence for significant $\Sigma(\text{SFR})/M$ - M_{200} or M_{200} - z correlations within the group and cluster samples separately. Hence the observed $\Sigma(\text{SFR})/M$ - z relation within each sample must be interpreted as a genuine redshift evolution of the $\Sigma(\text{SFR})/M$ of galaxy systems.

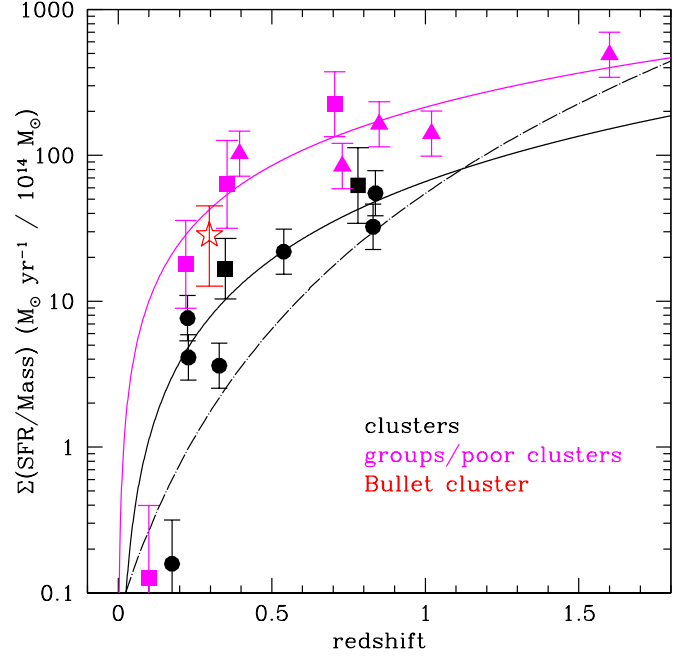


Fig. 2. $\Sigma(\text{SFR})/M$ -redshift relation for clusters (black symbols) and groups (magenta symbols). Square symbols, triangles, and dots identify, respectively, the COSMOS composite systems, the GOODS systems, and the remaining systems. The red star identifies the Bullet cluster. The black solid line shows the best fit $\Sigma(\text{SFR})/M$ - z relation for the cluster sample, excluding the Bullet cluster. The relation fitted to the data is of the type $\Sigma(\text{SFR})/M \propto z^{\alpha}$. The dashed line shows the relation, $\Sigma(\text{SFR})/M \propto (1+z)^{\alpha}$, of Bai et al. (2009) rescaled to the LIRG L_{IR} -regime and to the r_{200} region. The magenta solid lines shows the best fit for the sample of groups and poor clusters.

Groups appear to be characterized by higher $\Sigma(\text{SFR})/M$ values than clusters, at all redshifts, i.e. they show a higher SF activity than massive clusters. In this sense, when the sample of groups and clusters are considered together, $\Sigma(\text{SFR})/M$ does anticorrelate with the system M_{200} , as already found in previous studies (Finn et al. 2004, 2005; Homeier et al. 2005; Koyama et al. 2010).

The solid curves in Fig. 2 represent best-fit models to the observed $\Sigma(\text{SFR})/M$ - z relations, $\Sigma(\text{SFR})/M = (66 \pm 23) \times z^{1.77 \pm 0.36}$ for the cluster sample and $\Sigma(\text{SFR})/M = (213 \pm 44) \times z^{1.33 \pm 0.34}$ for the group sample. In Fig. 2 we also show as a dashed line the $\Sigma(\text{SFR})/M \propto (1+z)^{5.3}$ model proposed by Bai et al. (2009). We rescale their relation, which is built for $\Sigma(\text{SFR})$ computed down to a SFR limit of $2 M_{\odot} \text{ yr}^{-1}$, to our adopted LIRG limit, by using the IR luminosity function of Bai et al. (2009). Moreover, the $\Sigma(\text{SFR})$ in Bai et al.'s relation is evaluated within a radius of r_{500} , the radius corresponding to an overdensity equal to 500 times the critical density. To convert to our adopted radius r_{200} , we adopt a Navarro et al. (1997) model, with concentration $c=5$ to scale for the number of galaxies inside the two radii and derive the r_{500}/r_{200} ratio, and then use Fig. 7 in Bai et al. (2009) to account for the different fraction of IR-emitting galaxies at r_{500} and r_{200} . The modified relation of Bai et al. (2009) appears to fail to predict the rapid evolution of cluster $\Sigma(\text{SFR})/M$, as already suggested by Biviano et al. (2011).

3.2. Structures versus field

In Fig. 3 we compare the $\Sigma(\text{SFR})/M$ - z relation of galaxy systems with the corresponding relation for field galaxies (light blue shaded region and blue dashed line). The $\Sigma(\text{SFR})/M$ - z relation of field galaxies is obtained by dividing the observed Star Formation Rate Density (SFRD) of Magnelli et al. (2011, triangles) and the modeled SFRD of Gruppioni et al. (2011, dashed line), by the mean comoving density of the universe ($\Omega_m \times \rho_c$ where $\Omega_m = 0.3$ and ρ_c is the critical density of the Universe). Both SFRD have been evaluated only down to the SFR corresponding to the LIRG L_{IR} , via the Kennicutt relation.

The field SFRD has been estimated in large comoving volumes that include galaxy systems, voids, and isolated galaxies, and is thus representative of the general field galaxy population. According to the dark halo mass function of Jenkins et al. (2001), halos of $10^{11} - 10^{12} M_\odot$ give the main contribution to the dark matter budget at all redshifts. Thus, the $\Sigma(\text{SFR})/M$ of Fig. 3 can be considered as an effective estimate of the $\Sigma(\text{SFR})/M$ of galaxy-sized dark matter halos.

Observed and modeled $\Sigma(\text{SFR})/M$ are in very good agreement within the error bars. They increase from $z = 0$ to $z \sim 1$ where they reach a plateau.

The field $\Sigma(\text{SFR})/M$ - z relation lies above both the group and the cluster relations at $z \lesssim 0.2$. The field $\Sigma(\text{SFR})/M$ is more than an order of magnitude higher than those of Abell 2218 at $z = 0.175$ and of the composite COSMOS group at $z = 0.1$. At higher redshifts, group and field galaxy halos show comparable $\Sigma(\text{SFR})/M$. Possibly, the group $\Sigma(\text{SFR})/M$ lie above the field relation at $z \sim 1.6$, consistently with a reversal of the SFR-density relation observed by Elbaz et al. (2007), Cooper et al. (2008), and Popesso et al. (2011). However, this conclusion is based on a single group $\Sigma(\text{SFR})/M$ determination. Clusters have lower $\Sigma(\text{SFR})/M$ than field galaxy halos at all redshifts up to the last measured point at $z = 0.85$. A blind extrapolation of the best-fit cluster $\Sigma(\text{SFR})/M$ - z relation would suggest that clusters should display a higher SFR per unit mass than field galaxies at $z \gtrsim 2$. However, such an extrapolation is extremely uncertain with the present data and massive systems as the ones considered here should not even exist at such redshift according to Λ CDM hierarchical model predictions.

4. Discussion and conclusions

We find significant evidence for an evolution of the $\Sigma(\text{SFR})/M$ with z in clusters, groups, and the field. Both the cluster and the group $\Sigma(\text{SFR})/M$ increase monotonically with z and the field $\Sigma(\text{SFR})/M$ reaches a maximum at $z \gtrsim 1$.

The cluster $\Sigma(\text{SFR})/M$ evolution we find, appears to be faster, at least in the range $0 < z < 1$, compared to the evolutionary relation suggested by Geach et al. (2006); Bai et al. (2007, 2009); Koyama et al. (2010). This might be due to our higher- L_{IR} cut, if LIRGs evolve faster than less luminous IR-emitting galaxies. A faster evolution has already been suggested by Biviano et al. (2011), but only in the $z \lesssim 0.5$ range, while in our data there is no sign of a flattening of the $\Sigma(\text{SFR})/M$ - z relation for clusters above that redshift.

We confirm earlier indications (Finn et al. 2005; Bai et al. 2007; Koyama et al. 2010) that $\Sigma(\text{SFR})/M$ is lower for systems of higher mass, and we show for the first time that this is true at all redshifts from $z \sim 0$ to $z \sim 0.9$. This is true when we compare clusters to groups and the field. On the other hand, the group $\Sigma(\text{SFR})/M$ lies below the field relation only at $z \lesssim 0.2$. At higher redshifts, the group and the field $\Sigma(\text{SFR})/M$ become

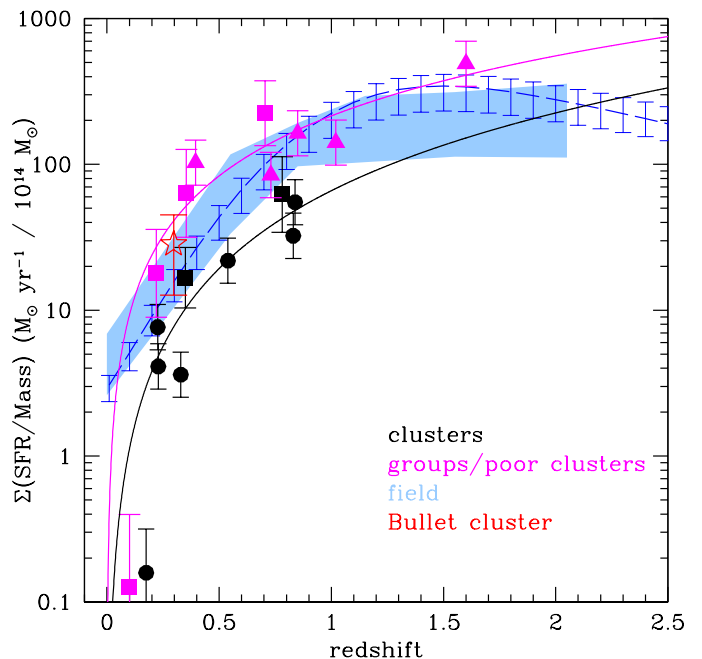


Fig. 3. The field $\Sigma(\text{SFR})/M$ -redshift relation from Magnelli et al. (2011) (light blue shaded region) and Gruppioni et al. (2011) (dashed blue line). The shading and error bars represent 1σ confidence levels. Other symbols/lines have the same meaning of the symbols as in Fig. 2

comparable. There is a hint of a reversal of the SFR activity vs. environment at $z \sim 1.6$, where the group $\Sigma(\text{SFR})/M$ lies above the field $\Sigma(\text{SFR})/M$ - z relation.

Our results appear to support a scenario in which the quenching of SF occurs earlier in galaxies embedded in more massive halos, i.e. first in clusters, then in groups, and finally in the field. This would be consistent with a “halo downsizing” effect, whereby massive halos evolve more rapidly than low mass halos (Neistein et al. 2006). Although in a narrow range of halo masses, the “halo downsizing” effect has already been observed in the stellar-to-total mass ratio vs. redshift relation by Foucaud et al. (2010).

What is causing the difference between the cluster and the group/field $\Sigma(\text{SFR})/M$ - z relation? The similarity of the field and the groups $\Sigma(\text{SFR})/M$ - z relations suggests that a SF quenching effect is taking place mostly after galaxies enter the cluster environment, and not in groups before they merge into more massive structures, as would be predicted by the pre-processing scenario (Zabludoff & Mulchaey 1998; Kodama et al. 2001; Balogh et al. 2011). We can therefore consider the field and group $\Sigma(\text{SFR})/M$ - z relation as indicating the normal galaxy evolution, and the cluster $\Sigma(\text{SFR})/M$ - z relation as the accelerated evolution experienced by galaxies following their accretion to more massive structures, as individuals or in groups. However, we point out that other differences may intervene between the star forming population of the groups and the field. Indeed, in agreement with our results, Tran et al. (2009) find consistent levels of star formation in the supergroup at $z = 0.37$ and the field population, but they also reveal a much higher fraction of early type galaxies among the SF galaxies of the group environment with respect to the field. Similar results are obtained

by Hwang & Park (2009). This could indicate a morphological transformation happening prior to the SF quenching effect.

Part of the observed evolution may come from internal, rather than external processes. In fact, most of the LIRGs in our sample are likely to be rather massive galaxies (as inferred from the almost linear, z -dependent, relation between galaxy SFRs and stellar masses of Elbaz et al. 2007), and according to Peng et al. (2010) massive galaxies evolve mostly because of an internally driven process, called 'mass quenching', caused perhaps by feedback from active galactic nuclei. But since this process is unlikely to be more efficient in quenching SF of massive galaxies in clusters than in other environments, we need to consider an additional quenching process that would operate only in the cluster environment.

Two obvious candidates for producing this additional quenching, are ram-pressure stripping (Gunn & Gott 1972) and starvation (Larson et al. 1980). Ram-pressure stripping is a fast process (Abadi et al. 1999) and is effective only in galaxy systems where the gas density is high, i.e. in clusters. However, ram-pressure stripping seems ruled out by the presence of LIRGs contributed by the infalling group (the "bullet") in the Bullet cluster. The group LIRG contribution is probably the reason of the position of the Bullet cluster in the $\Sigma(\text{SFR})/M-z$ plot, intermediate between that of clusters and groups (Chung et al. 2010). If rapid ram-pressure stripping was a major star formation quenching process, the group LIRGs could have had their star formation quenched already, given that the cluster-group collision happened ~ 250 Myr ago (Springel & Farrar 2007).

Starvation, caused by the removal of the hot gas halo reservoirs of galaxies, is a more likely candidate given that we see an accelerated evolution (relative to the field) both in clusters and in groups (Kawata & Mulchaey 2008; Bekki 2009). The removal of galaxy hot gas reservoirs inducing starvation can be caused by tidal galaxy-galaxy encounters or by the interaction with the intra-cluster/intra-group medium. Starvation should proceed more effectively in higher (galaxy or gas) density regions, hence it should quench SF earlier in cluster than in group galaxies, as we observe.

In order to better constrain these evolutionary scenarios it is important to extend the analysis of the $\Sigma(\text{SFR})/M-z$ relation to even higher redshifts, where we might expect to see a reversal of the environment dependence as we approach the epoch when galaxies in dense environments underwent their first major episodes of SF. In the near future we plan to use new Herschel PACS observations of 6 poor and rich clusters at $1.4 < z < 1.9$ to explore this issue.

Acknowledgements. PACS has been developed by a consortium of institutes led by MPE (Germany) and including UVIE (Austria); KUL, CSL, IMEC (Belgium); CEA, OAMP (France); MPIA (Germany); IFSI, OAP/AOT, OAA/CAISMI, LENS, SISSA (Italy); IAC (Spain). This development has been supported by the funding agencies BMVIT (Austria), ESA-PRODEX (Belgium), CEA/CNES (France), DLR (Germany), ASI (Italy), and CICYT/MCYT (Spain).

We gratefully acknowledge the contributions of the entire COSMOS collaboration consisting of more than 100 scientists. More information about the COSMOS survey is available at <http://www.astro.caltech.edu/~cosmos>.

This research has made use of NASA's Astrophysics Data System, of NED, which is operated by JPL/Caltech, under contract with NASA, and of SDSS, which has been funded by the Sloan Foundation, NSF, the US Department of Energy, NASA, the Japanese Monbukagakusho, the Max Planck Society, and the Higher Education Funding Council of England. The SDSS is managed by the participating institutions (www.sdss.org/collaboration/credits.html).

References

Abadi, M. G., Moore, B., & Bower, R. G. 1999, *MNRAS*, 308, 947

- Abazajian, K. N., Adelman-McCarthy, J. K., Agüeros, M. A., et al. 2009, *ApJS*, 182, 543
- Abell, G. O., Corwin, Jr., H. G., & Olowin, R. P. 1989, *ApJS*, 70, 1
- Bai, L., Marcellac, D., Rieke, G. H., et al. 2007, *ApJ*, 664, 181
- Bai, L., Rieke, G. H., Rieke, M. J., Christlein, D., & Zabludoff, A. I. 2009, *ApJ*, 693, 1840
- Balogh, M. L., McGee, S. L., Wilman, D. J., et al. 2011, *MNRAS*, 412, 2303
- Barger, A. J., Cowie, L. L., & Wang, W.-H. 2008, *ApJ*, 689, 687
- Barrena, R., Biviano, A., Ramella, M., Falco, E. E., & Seitz, S. 2002, *A&A*, 386, 816
- Bauer, F. E., Alexander, D. M., Brandt, W. N., et al. 2002, *AJ*, 123, 1163
- Beers, T. C., Flynn, K., & Gebhardt, K. 1990, *AJ*, 100, 32
- Bekki, K. 2009, *MNRAS*, 399, 2221
- Berta, S., Magnelli, B., Lutz, D., et al. 2010, *A&A*, 518, L30
- Biviano, A., Fadda, D., Durret, F., Edwards, L. O. V., & Marleau, F. 2011, *A&A*, 532, A77
- Biviano, A., Murante, G., Borgani, S., et al. 2006, *A&A*, 456, 23
- Brusa, M., Fiore, F., Santini, P., et al. 2009, *A&A*, 507, 1277
- Butcher, H. & Oemler, Jr., A. 1978, *ApJ*, 219, 18
- Butcher, H. & Oemler, Jr., A. 1984, *ApJ*, 285, 426
- Chary, R. & Elbaz, D. 2001, *ApJ*, 556, 562
- Chung, S. M., Gonzalez, A. H., Clowe, D., Markevitch, M., & Zaritsky, D. 2010, *ApJ*, 725, 1536
- Cimatti, A., Robberto, M., Baugh, C., et al. 2008, *Experimental Astronomy*, 37
- Coia, D., McBreen, B., Metcalfe, L., et al. 2005, *A&A*, 431, 433
- Cooper, M. C., Newman, J. A., Weiner, B. J., et al. 2008, *MNRAS*, 383, 1058
- Demarco, R., Rosati, P., Lidman, C., et al. 2005, *A&A*, 432, 381
- Dressler, A. 1980, *ApJ*, 236, 351
- Dressler, A. & Gunn, J. E. 1983, *ApJ*, 270, 7
- Dressler, A., Oemler, A. J., Couch, W. J., et al. 1997, *ApJ*, 490, 577
- Dressler, A., Smail, I., Poggianti, B. M., et al. 1999, *ApJS*, 122, 51
- Elbaz, D., Daddi, E., Le Borgne, D., et al. 2007, *A&A*, 468, 33
- Elbaz, D., Dickinson, M., Hwang, H. S., et al. 2011, 1105.2537
- Fadda, D., Biviano, A., Marleau, F. R., Storrie-Lombardi, L. J., & Durret, F. 2008, *ApJ*, 672, L9
- Fasano, G., Poggianti, B. M., Couch, W. J., et al. 2000, *ApJ*, 542, 673
- Ferrari, C., Benoist, C., Maurogordato, S., Cappi, A., & Slezak, E. 2005, *A&A*, 430, 19
- Finn, R. A., Zaritsky, D., & McCarthy, Jr., D. W. 2004, *ApJ*, 604, 141
- Finn, R. A., Zaritsky, D., McCarthy, Jr., D. W., et al. 2005, *ApJ*, 630, 206
- Fisher, D., Fabricant, D., Franx, M., & van Dokkum, P. 1998, *ApJ*, 498, 195
- Foucaud, S., Conselice, C. J., Hartley, W. G., et al. 2010, *MNRAS*, 406, 147
- Gavazzi, G., Boselli, A., Pedotti, P., Gallazzi, A., & Carrasco, L. 2002, *A&A*, 396, 449
- Geach, J. E., Smail, I., Ellis, R. S., et al. 2006, *ApJ*, 649, 661
- Gilli, R., Cimatti, A., Daddi, E., et al. 2003, *ApJ*, 592, 721
- Girardi, M., Biviano, A., Giuricin, G., Mardirossian, F., & Mezzetti, M. 1993, *ApJ*, 404, 38
- Gómez, P. L., Nichol, R. C., Miller, C. J., et al. 2003, *ApJ*, 584, 210
- Grazian, A., Fontana, A., de Santis, C., et al. 2006, *A&A*, 449, 951
- Gruppioni, C., Pozzi, F., Andreani, P., et al. 2010, *A&A*, 518, L27
- Gruppioni, C., Pozzi, F., Zamorani, G., & Vignali, C. 2011, 1105.1955
- Gunn, J. E. & Gott, J. R. 1972, *ApJ*, 176, 1
- Haines, C. P., Smith, G. P., Egami, E., et al. 2009, *ApJ*, 704, 126
- Harrison, E. R. & Noonan, T. W. 1979, *ApJ*, 232, 18
- Hashimoto, Y., Oemler, A. J., Lin, H., & Tucker, D. L. 1998, *ApJ*, 499, 589
- Hayashi, M., Kodama, T., Koyama, Y., Tadaki, K.-I., & Tanaka, I. 2011, *MNRAS*, 415, 2670
- Homeier, N. L., Demarco, R., Rosati, P., et al. 2005, *ApJ*, 621, 651
- Hwang, H. S. & Park, C. 2009, *ApJ*, 700, 791
- Ilbert, O., Salvato, M., Le Flocc'h, E., et al. 2010, *ApJ*, 709, 644
- Jenkins, A., Frenk, C. S., White, S. D. M., et al. 2001, *MNRAS*, 321, 372
- Johnson, O., Best, P. N., & Almaini, O. 2003, *MNRAS*, 343, 924
- Kawata, D. & Mulchaey, J. S. 2008, *ApJ*, 672, L103
- Kodama, T., Balogh, M. L., Smail, I., Bower, R. G., & Nakata, F. 2004, *MNRAS*, 354, 1103
- Kodama, T., Smail, I., Nakata, F., Okamura, S., & Bower, R. G. 2001, *ApJ*, 562, L9
- Koyama, Y., Kodama, T., Shimasaku, K., et al. 2010, *MNRAS*, 403, 1611
- Kurk, J., Cimatti, A., Zamorani, G., et al. 2008, in *Astronomical Society of the Pacific Conference Series*, Vol. 399, *Panoramic Views of Galaxy Formation and Evolution*, ed. T. Kodama, T. Yamada, & K. Aoki, 332
- Larson, R. B., Tinsley, B. M., & Caldwell, C. N. 1980, *ApJ*, 237, 692
- Le Borgne, J. F., Pello, R., & Sanahuja, B. 1992, *A&AS*, 95, 87
- Le Fèvre, O., Vettolani, G., Paltani, S., et al. 2004, *A&A*, 428, 1043
- Le Flocc'h, E., Aussel, H., Ilbert, O., et al. 2009, *ApJ*, 703, 222
- Lewis, I., Balogh, M., De Propriis, R., et al. 2002, *MNRAS*, 334, 673
- Lilly, S. J., Le Brun, V., Maier, C., et al. 2009, *ApJS*, 184, 218

- Lilly, S. J., Le Fèvre, O., Renzini, A., et al. 2007, *ApJS*, 172, 70
- Lutz, D., Mainieri, V., Rafferty, D., et al. 2010, *ApJ*, 712, 1287
- Lutz, D., Poglitsch, A., Altieri, B., et al. 2011, 1106.3285
- Madau, P., Pozzetti, L., & Dickinson, M. 1998, *ApJ*, 498, 106
- Magnelli, B., Elbaz, D., Chary, R. R., et al. 2011, *A&A*, 528, A35
- Mamon, G. A., Biviano, A., & Murante, G. 2010, *A&A*, 520, A30
- Markevitch, M., Gonzalez, A. H., Clowe, D., et al. 2004, *ApJ*, 606, 819
- Mauduit, J.-C. & Mamon, G. A. 2007, *A&A*, 475, 169
- Miller, N. A. & Owen, F. N. 2003, *AJ*, 125, 2427
- Moore, B., Katz, N., Lake, G., Dressler, A., & Oemler, Jr., A. 1996, *Nature*, 379, 613
- Moran, S. M., Ellis, R. S., Treu, T., et al. 2005, *ApJ*, 634, 977
- Moran, S. M., Ellis, R. S., Treu, T., et al. 2007, *ApJ*, 671, 1503
- Navarro, J. F., Frenk, C. S., & White, S. D. M. 1997, *ApJ*, 490, 493
- Neistein, E., van den Bosch, F. C., & Dekel, A. 2006, *MNRAS*, 372, 933
- Netzer, H., Lutz, D., Schweitzer, M., et al. 2007, *ApJ*, 666, 806
- Nordon, R., Lutz, D., Berta, S., et al. 2011, 1106.1186
- Park, C. & Hwang, H. S. 2009, *ApJ*, 699, 1595
- Patel, S. G., Holden, B. P., Kelson, D. D., Illingworth, G. D., & Franx, M. 2009, *ApJ*, 705, L67
- Peng, Y., Lilly, S. J., Kovač, K., et al. 2010, *ApJ*, 721, 193
- Pimbblet, K. A. 2003, *PASA*, 20, 294
- Pipino, A. & Matteucci, F. 2004, *MNRAS*, 347, 968
- Poggianti, B. M., Bridges, T. J., Komiyama, Y., et al. 2004, *ApJ*, 601, 197
- Poggianti, B. M., Smail, I., Dressler, A., et al. 1999, *ApJ*, 518, 576
- Polletta, M., Tajer, M., Maraschi, L., et al. 2007, *ApJ*, 663, 81
- Popesso, P., Dickinson, M., Nonino, M., et al. 2009, *A&A*, 494, 443
- Popesso, P., Rodighiero, G., Saintonge, A., et al. 2011, 1104.1094
- Porter, S. C., Raychaudhury, S., Pimbblet, K. A., & Drinkwater, M. J. 2008, *MNRAS*, 388, 1152
- Postman, M., Franx, M., Cross, N. J. G., et al. 2005, *ApJ*, 623, 721
- Prescott, M. K. M., Impey, C. D., Cool, R. J., & Scoville, N. Z. 2006, *ApJ*, 644, 100
- Rodighiero, G., Cimatti, A., Gruppioni, C., et al. 2010, *A&A*, 518, L25
- Saintonge, A., Tran, K.-V. H., & Holden, B. P. 2008, *ApJ*, 685, L113
- Sanders, D. B., Salvato, M., Aussel, H., et al. 2007, *ApJS*, 172, 86
- Santini, P., Fontana, A., Grazian, A., et al. 2009, *A&A*, 504, 751
- Smith, G. P., Treu, T., Ellis, R. S., Moran, S. M., & Dressler, A. 2005, *ApJ*, 620, 78
- Springel, V. & Farrar, G. R. 2007, *MNRAS*, 380, 911
- Temporin, S., Duc, P., Ilbert, O., & XMM-LSS/SWIRE collaboration. 2009, *Astronomische Nachrichten*, 330, 915
- Tran, K.-V. H., Franx, M., Illingworth, G. D., et al. 2007, *ApJ*, 661, 750
- Tran, K.-V. H., Saintonge, A., Moustakas, J., et al. 2009, *ApJ*, 705, 809
- Trump, J. R., Impey, C. D., McCarthy, P. J., et al. 2007, *ApJS*, 172, 383
- Yahil, A. & Vidal, N. V. 1977, *ApJ*, 214, 347
- Yee, H. K. C., Ellingson, E., Abraham, R. G., et al. 1996, *ApJS*, 102, 289
- Zabludoff, A. I. & Mulchaey, J. S. 1998, *ApJ*, 498, L5